11. Softening-Hardening Material Model

Experimental evidence indicates that the plastic deformation in soils starts from the early stages of loading. To capture such behavior in a constitutive model the typical elasto-perfect plastic models are not adequate. It requires constitutive models that utilize a hardening law after initial yielding.

The Softening-Hardening Model in *RS2* and *RS3* has been developed to meet the abovementioned need. The model can utilize up to three yield surfaces that includes deviatoric (shear), volumetric (cap) and tension cut off. The yield surfaces and hardening characteristics of this model are illustrated in Figure 11.1 in p-q plane and Figures 11.2 and11.3 show the yield surfaces in 3D stress space. Based on the formulations of this model it is apt to say that this model has three different mechanisms, i.e., deviatoric, volumetric and tension cutoff. The model is designed to be very flexible with its numerous options and formulations. It can take advantage of the various options of elastic behavior that were presented in the Chapter 2. In its simplest form this model can be equivalent to Mohr-Coulomb model, with activation of a few options can replace the Duncan-Chang model or the ChSoil model, and by taking advantage of more options, including nonlinear elasticity, it can be equivalent to the Hardening Soil, Double yield and CySoil model.

The formulations of these three mechanisms, definition of yield surfaces and their corresponding plastic potential and hardening law are presented in the following sections (Pietruszczak 2010).

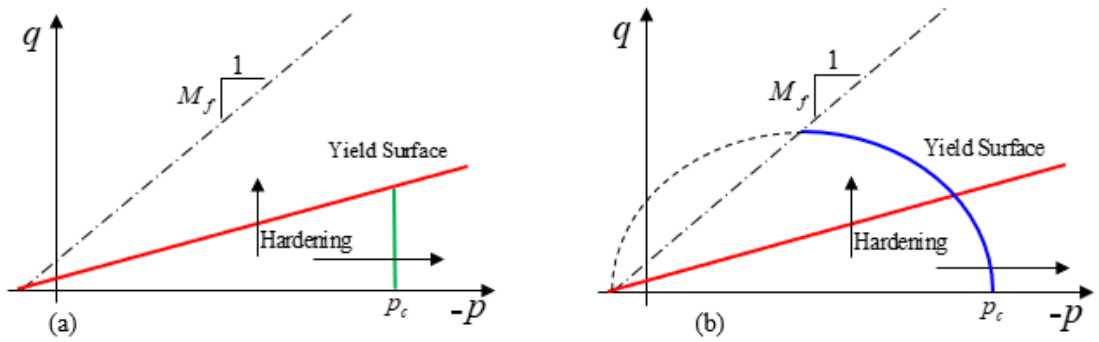

Figure 0.1. The yield surfaces of the Softening-Hardening model; a) Deviatoric yield surface (red) and the vertical cap (green); b) Deviatoric yield surface (red) and elliptical cap (blue)

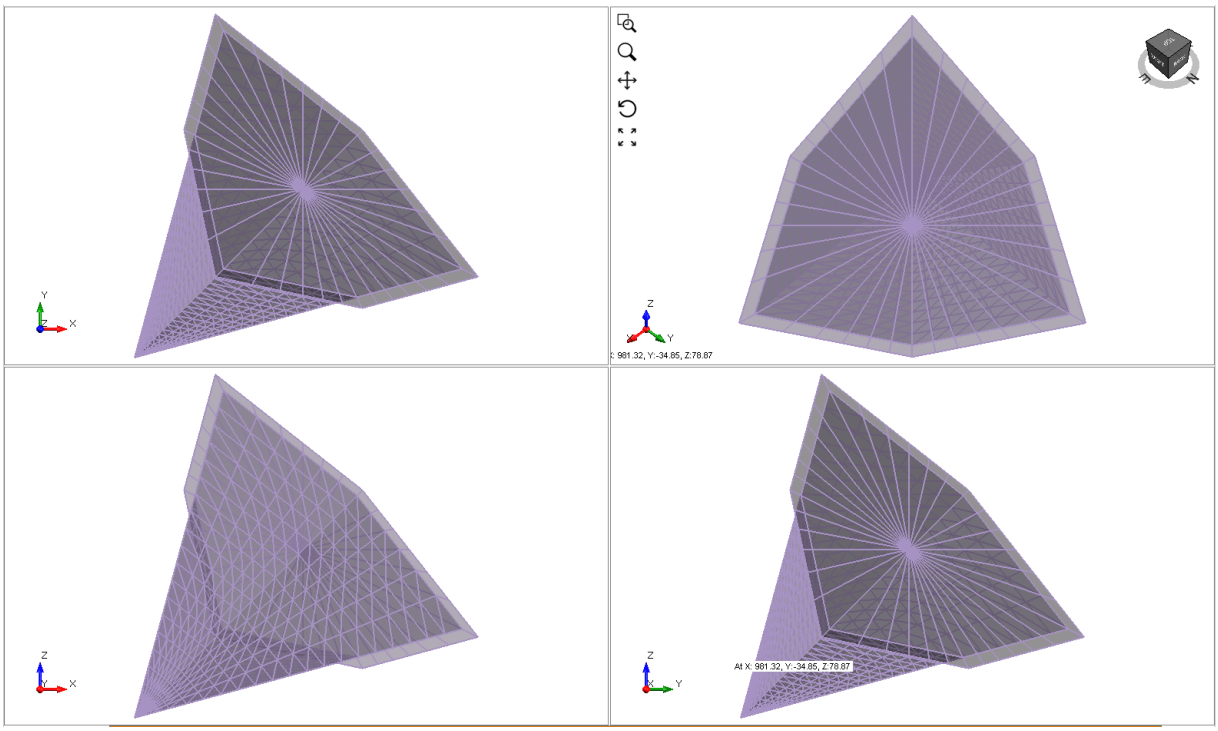

Figure 11.2. Yield surface of Softening-Hardening model with vertical cap in 3D stress space

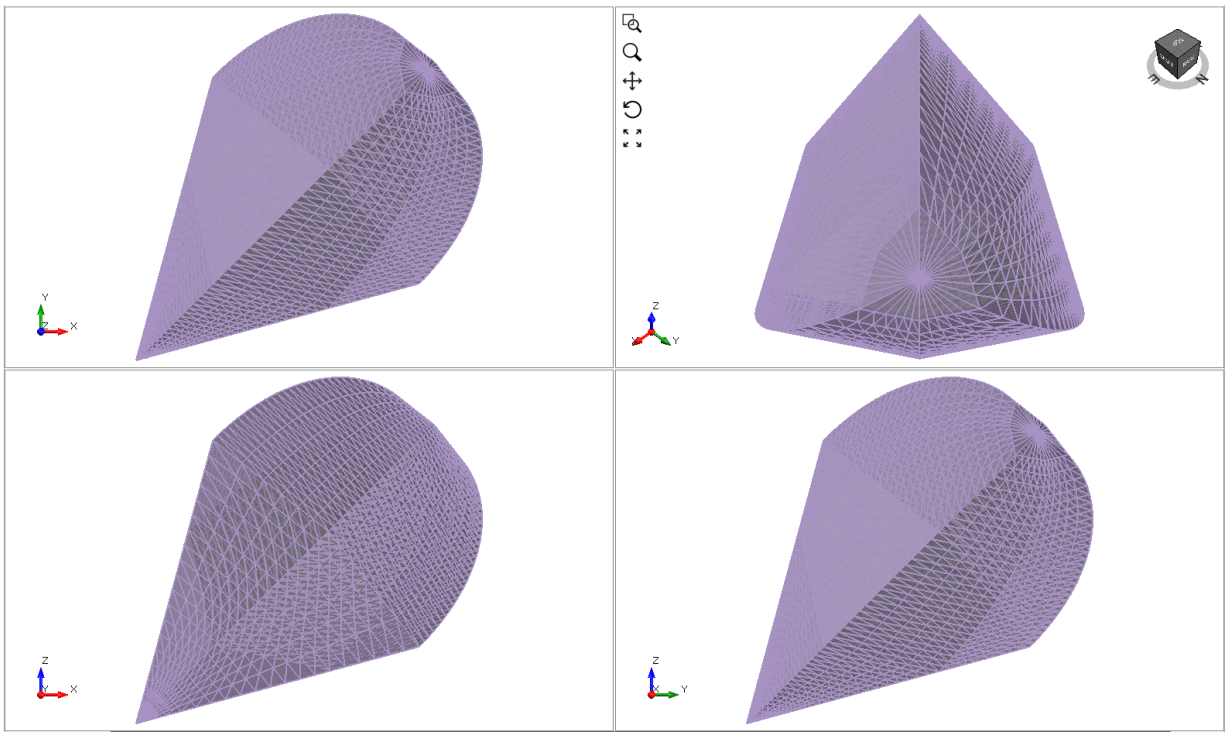

Figure 11.3. Yield surface of Softening-Hardening model with elliptical cap in 3D stress space

11.1 Deviatoric Hardening Mechanism

The deviatoric mechanism is the core of this model and its yield surface is very similar to the yield surface of the Mohr-Coulomb model.

The equation for the Mohr-Coulomb yield surface using the (p, q, θ) invariants is given by

$$F_s = q + M\left(p - \frac{c}{\tan\varphi}\right) = 0 \tag{0.1}$$

where

$$M = \frac{3\sin\varphi}{\sqrt{3}\cos\theta - \sin\theta\sin\varphi} \tag{0.2}$$

The hardening for this yield surface is considered for the mobilized friction angle (and cohesion) and it is attributed to plastic distortion. The equations above are rewritten as:

$$F_s = q + M\left(p - \frac{c}{\tan\varphi_f}\right) = 0 \quad , \quad M = \frac{3\sin\varphi}{\sqrt{3}\cos\theta - \sin\theta\sin\varphi} \tag{0.3}$$

In above φ_f is the ultimate/failure friction angle and c and φ are the mobilized cohesion and friction angle respectively.

There are two types of hardening law considered for this model. The first one uses a relationship between $\tan\varphi$ and the deviatoric plastic strain presented in equation 11.4.

$$\tan\varphi = \tan\varphi_f \frac{\varepsilon_q^p}{\varepsilon_q^p + A} \tag{0.4}$$

where ε_q^p is the deviatoric plastic strain that is generated by the deviatoric mechanism only, and A is a positive and constant hardening parameter.

The second hardening law uses custom tabular piecewise linear values for the mobilized friction angle and cohesion with deviatoric plastic strain $\left(\varepsilon_q^p, \varphi\right)$ & $\left(\varepsilon_q^p, c\right)$.

The first hardening law is quite simple and uses only one additional parameter on top of what is required for a simple Mohr-Coulomb material model. The second one gives the user the flexibility to define any kind of hardening/softening rule that meets their material modelling needs.

Two options are considered for the plastic potential of the deviatoric hardening yield surface. The first one is very similar to that of the Mohr-Coulomb model where a dilation angle (ψ_f) is defined and controls the dilation tendency of the material. The only difference here is that the defined dilation angle is the dilation angle at failure, where the mobilized friction angle reaches its ultimate value $(\varphi = \varphi_f)$. The actual dilation angle used during plastic flow is proportional to the ratio of the mobilized friction angle to its failure value. The plastic potential function for this option is given in equation 11.6.

$$\psi = \psi_f \frac{\varphi}{\varphi_f} \tag{0.5}$$

$$Q_s = q + M_\psi p = const \quad , \quad M_\psi = \frac{3\sin\psi}{\sqrt{3}\cos\theta - \sin\theta\sin\psi} \tag{0.6}$$

The other option for plastic potential is to define a compaction-dilation angle in such a way that where the mobilized friction angle (φ) is less than this angle (ψ) the volumetric plastic strain is positive (compaction) and when the mobilized friction angle is greater than ψ the volumetric plastic strain is negative (dilation). The plastic potential function for this case is:

$$Q_s = q - M_\psi p ln\left(\frac{-p}{p_c}\right) = const \quad , \quad M = \frac{3\sin\psi}{\sqrt{3}\cos\theta - \sin\theta\sin\psi} \tag{0.7}$$

When used solely, this mechanism, can be a good alternative to the Duncan-Chang model and does not have its short fallings. This is also a good alternative for the ChSoil model, and using the various options for nonlinear elasticity and the flexibility of the tabular hardening rule gives flexibilities to the behaviors this mechanism can simulate. The tabular hardening option can also be used to simulate a softening behavior. Note that simulating the softening behavior as a material behavior is not recommended since it will make the finite element solution results unreliable and mesh dependent. The apparent softening behavior that is observed in laboratory tests is to be simulated, for example, by taking advantage of more complex formulations that can deal with strain localization shear banding.

11.2 Volumetric Hardening Mechanism

The main role of the volumetric mechanism (cap) is to close the elastic domain in space $(p - q)$ on the hydrostatic (p) axis and simulate the densification/compaction of the material. Addition of the cap yield is optional in this model but when activated there are two options for the it, vertical cap and elliptical cap.

The yield surface of the vertical cap is defined as follows.

$$F_c = p + p_c = 0 \tag{0.8}$$

where p_c is the location of the intersection of this yield surface with the p axis. With activation of the vertical cap this model is equivalent to Double-Yield model.

The elliptical cap is very similar to the yield surface of the modified Cam-Clay model with an offset to consider the cohesion that was defined in the deviatoric mechanism.

$$F_c = \left(\frac{q}{M_f}\right)^2 + \left(p - \frac{c}{tan\varphi_f}\right)(p + p_c) = 0 \quad , \quad M_f = \frac{3\sin\varphi_f}{\sqrt{3}\cos\theta - \sin\theta\sin\varphi_f} \tag{0.9}$$

Activation of the elliptical cap makes this model similar to the Hardening Soil and CySoil models. The difference between the cap in this model with the cap in the Hardening Soil and CySoil is that the apex of this cap tracks the ultimate shear yield surface. This cap is similar to the yield surface of modified Cam Clay model in that at ultimate shear failure the cap will be at critical state condition and will not generate any compaction.

The hardening for these yield surfaces is considered for p_c and it is attributed to volumetric plastic strain. The built in function for the hardening follows the same hardening law as in the Modified Cam-Clay model:

$$(p_c)_{n+1} = (p_c)_n \exp\left(\frac{\Delta\varepsilon_v^p}{\lambda}\right) \tag{0.10}$$

where n is the step number, ε_v^p is the volumetric plastic strain, and λ is the difference between the slope of normal consolidation line and the swelling line. This hardening rule is similar to the hardening rule of Cam Clay model.

Tabular hardening law which uses custom tabular piecewise linear values for p_c versus volumetric plastic strain (ε_v^p, p_c) is also available for this model. This option will give the flexibility to use any other hardening law for the cap, e.g., the hardening rules used in Hardening Soil or CySoil models.

The flow rule is associated for this yield surface.

11.3 Tension Cut-Off

This mechanism is to incorporate the tensile strength of the material to this model. In this mechanism the minor principal stress is limited to the tensile strength of the material. The flow rule is associated and the mechanism has no hardening.

$$F_T = \sigma_3 - T = 0 \tag{0.11}$$

In above T is the tensile strength of the material.

11.4 Examples

Figure 11.4 and 11.5 shows the experimental and numerical results of drained triaxial tests on loose and dense Hostun sand respectively. The experimental results of drained triaxial test on dense and loose Hostun sand are depicted from Schanz and Vermeer (1996). All the triaxial tests start from an initial hydrostatic confinement of 300 kPa. The numerical results are obtained by using only the deviatoric hardening mechanism with compaction-dilation option for the plastic flow and a linear elastic behavior. The hardening rule for the loose Hostun sand uses the form that is presented in Equation 11.4. The Dense sand is simulated once by using the same hardening rule as in Equation 11.4 and by using a tabular function to capture the softening behavior. The model parameters are presented next to the graphs. Stress paths of the drained tests include variations of axial stress and volumetric strain with increasing axial strain, variation of deviatoric stress with deviatoric strain and the stress path in p-q plane. The ultimate yield surface of the deviatoric mechanism is also shown in the p-q plane. The simulated behavior captures the hardening behavior and the gradual compaction of loose sand. In the case of dense sand, the initial compaction that

follows with dilation is fully captured with the help of the appropriate choice of plastic flow option. The hardening of dense sand is captured by both options of the hardening rules that are used here, but only the tabular hardening option can capture softening behavior.

Figure 11.6 shows the experimental and numerical results of an undrained triaxial test on loose Banding sand. The experimental results of undrained triaxial test on Banding sand are depicted Castro (1969). The triaxial test starts at the initial confinement of 400 kPa. The generation of excess pore water pressure in loose sands under undrained conditions can lead to static liquefaction and total loss of strength. This phenomenon can be observed in Figure 6. The simulation results presented in this figure are in good agreement with the experimental results.

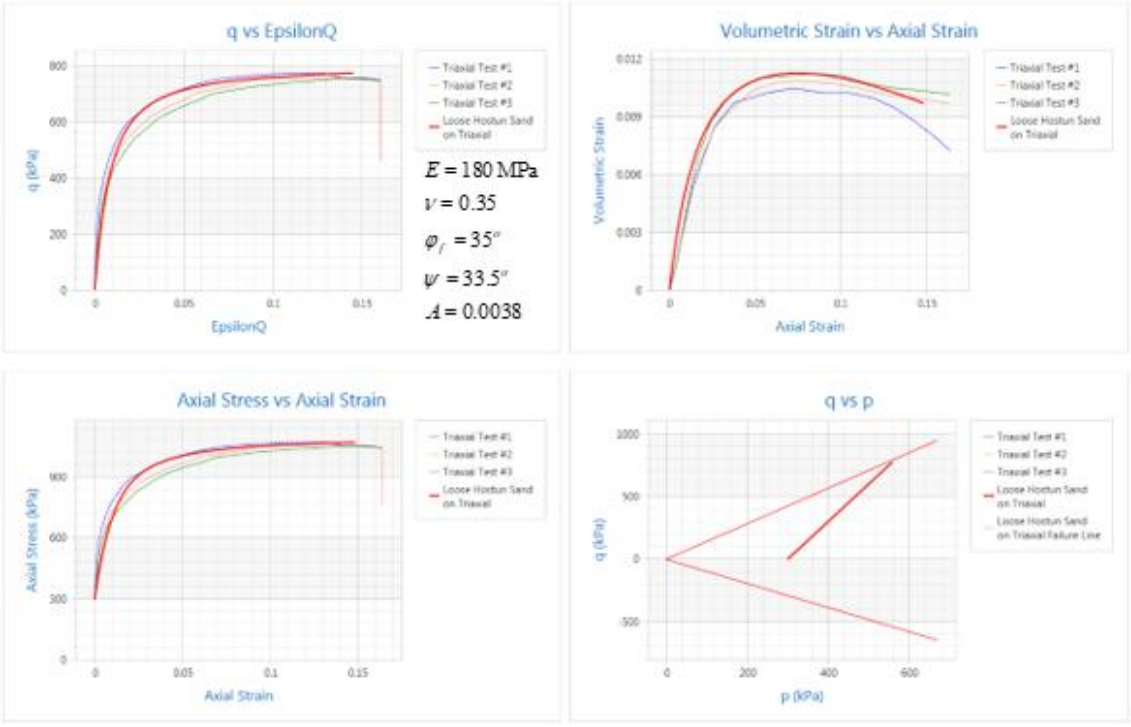

Figure 11.4. Stress paths of drained triaxial tests on loose Hostun sand

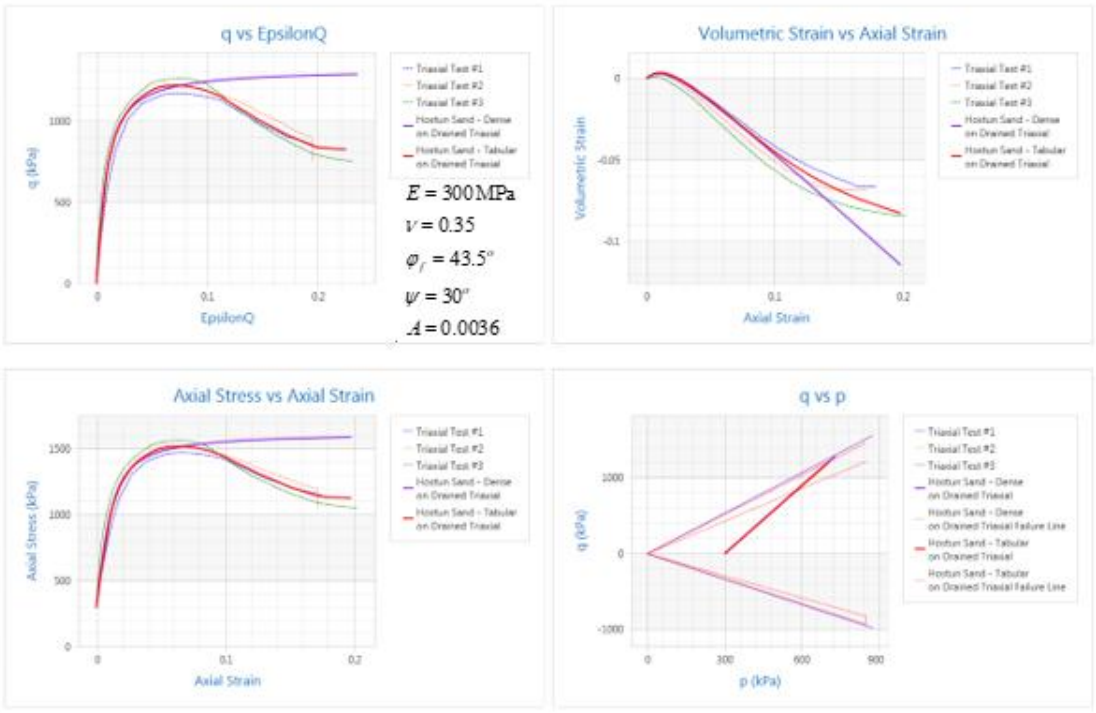

Figure 11.5. Stress paths of drained triaxial tests on dense Hostun sand

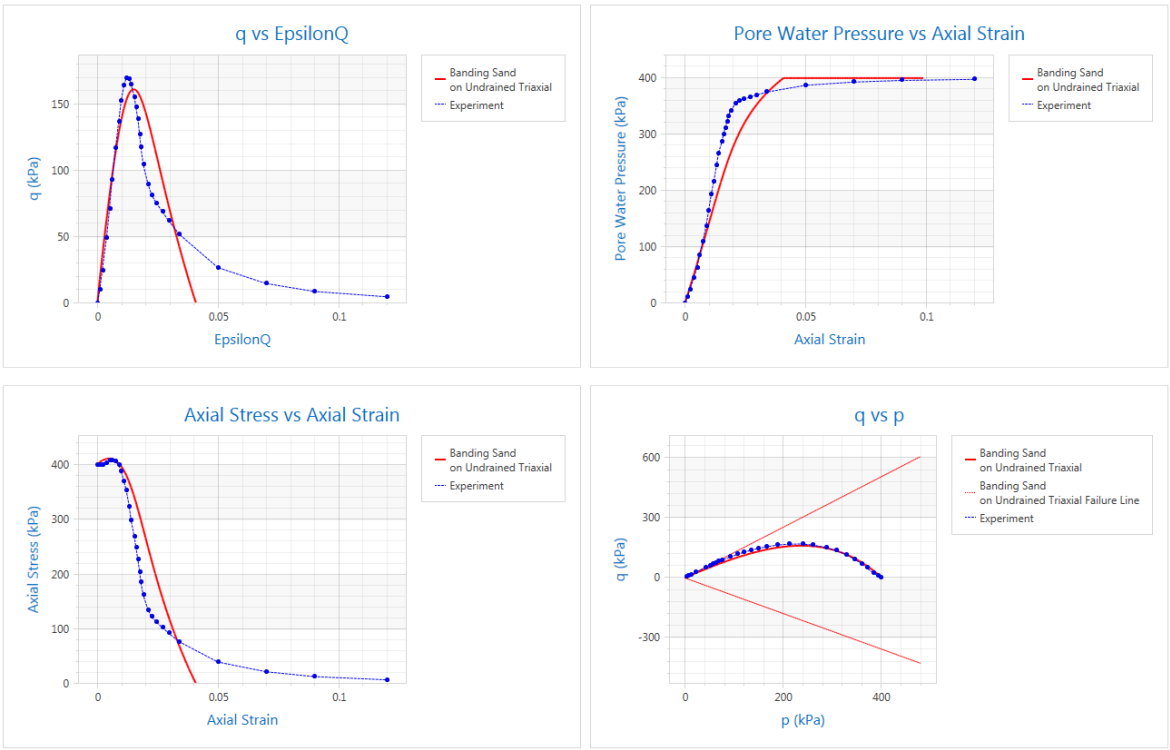

Figure 11.5. Stress paths of undrained triaxial tests on Banding sand

References

Castro, G. (1969). Liquefaction of sands, Harvard Soil Mechanics Series, No.81, Pierce Hall.

Pietruszczak, S. (2010). Fundamentals of Plasticity in Geomechanics. CRC Press.

Schanz, T. and Vermeer, P.A. (1996). Angles of friction and dilatancy of sand, Géotechnique 46(1): 145-151.